BIOCHEMISTRY
including biophysical chemistry & molecular biology
Article

Biochemistry **2010,** *49,* 10381–10393 10381
DOI: 10.1021/bi100733q

Important Roles of Tyr43 at the Putative Heme Distal Side in the Oxygen Recognition and Stability of the Fe(II)−O_2 Complex of YddV, a Globin-Coupled Heme-Based Oxygen Sensor Diguanylate Cyclase[†]

Kenichi Kitanishi,[‡] Kazuo Kobayashi,[§] Yuriko Kawamura,[‡] Izumi Ishigami,[∥] Takashi Ogura,[∥] Kyosuke Nakajima,[‡] Jotaro Igarashi,[‡] Atsunari Tanaka,[‡,⊥] and Toru Shimizu*[,‡]

[‡]*Institute of Multidisciplinary Research for Advanced Materials, Tohoku University, Katahira, Aoba-ku, Sendai 980-8577, Japan,* [§]*Institute of Scientific and Industrial Research, Osaka University, Mihogaoka 8-1, Ibaraki, Osaka 567-0047, Japan, and* [∥]*Department of Life Science, Graduate School of Life Science, University of Hyogo, Kamigori-cho, Ako-gun, Hyogo 678-1297, Japan.* [⊥]*Present address: The Wistar Institute, Philadelphia, PA 19104.*

Received May 10, 2010; Revised Manuscript Received November 9, 2010

ABSTRACT: YddV from *Escherichia coli* (*Ec*) is a novel globin-coupled heme-based oxygen sensor protein displaying diguanylate cyclase activity in response to oxygen availability. In this study, we quantified the turnover numbers of the active [Fe(III), 0.066 min^{-1}; Fe(II)−O_2 and Fe(II)−CO, 0.022 min^{-1}] [Fe(III), Fe(III)−protoporphyrin IX complex; Fe(II), Fe(II)−protoporphyrin IX complex] and inactive forms [Fe(II) and Fe(II)−NO, < 0.01 min^{-1}] of YddV for the first time. Our data indicate that the YddV reaction is the rate-determining step for two consecutive reactions coupled with phosphodiesterase *Ec* DOS activity on cyclic di-GMP (c-di-GMP) [turnover number of *Ec* DOS−Fe(II)−O_2, 61 min^{-1}]. Thus, O_2 binding and the heme redox switch of YddV appear to be critical factors in the regulation of c-di-GMP homeostasis. The redox potential and autoxidation rate of heme of the isolated heme domain of YddV (YddV-heme) were determined to be −17 mV versus the standard hydrogen electrode and 0.0076 min^{-1}, respectively. The Fe(II) complexes of Y43A and Y43L mutant proteins (residues at the heme distal side of the isolated heme-bound globin domain of YddV) exhibited very low O_2 affinities, and thus, their Fe(II)−O_2 complexes were not detected on the spectra. The O_2 dissociation rate constant of the Y43W protein was > 150 s^{-1}, which is significantly larger than that of the wild-type protein (22 s^{-1}). The autoxidation rate constants of the Y43F and Y43W mutant proteins were 0.069 and 0.12 min^{-1}, respectively, which are also markedly higher than that of the wild-type protein. The resonance Raman frequencies representing ν_{Fe-O_2} (559 cm^{-1}) of the Fe(II)−O_2 complex and ν_{Fe-CO} (505 cm^{-1}) of the Fe(II)−CO complex of Y43F differed from those (ν_{Fe-O_2}, 565 cm^{-1}; ν_{Fe-CO}, 495 cm^{-1}) of the wild-type protein, suggesting that Tyr43 forms hydrogen bonds with both O_2 and CO molecules. On the basis of the results, we suggest that Tyr43 located at the heme distal side is important for the O_2 recognition and stability of the Fe(II)−O_2 complex, because the hydroxyl group of the residue appears to interact electrostatically with the O_2 molecule bound to the Fe(II) complex in YddV. Our findings clearly support a role of Tyr in oxygen sensing, and thus modulation of overall conversion from GTP to pGpG via c-di-GMP catalyzed by YddV and *Ec* DOS, which may be applicable to other globin-coupled oxygen sensor enzymes.

Cyclic di-GMP [bis(3′−5′)-cyclic dimeric guanosine monophosphate (c-di-GMP)][1] is an important second messenger in bacteria (*1*, *2*). Synthesis [diguanylate cyclase (DGC)] and degradation [phosphodiesterase (PDE)] of c-di-GMP are triggered by initial signals, such as phosphorylation, ion binding, DNA binding, light illumination, gas binding, and other chemical and physical stimuli (*3*−*7*). In contrast, output signals in the form of increased or decreased concentrations of c-di-GMP [or linear-di-GMP or pGpG, a degraded form of c-di-GMP produced by phosphodiesterase (PDE)] regulate numerous physiological functions, including motility, virulence, development, cell−cell communication, and biofilm formation (*1*−*7*). Accordingly, modulation of the c-di-GMP concentration is critical for the maintenance or survival of bacterial cells under various stress conditions.

In the *Escherichia coli* genome, *yddV* and *dos* genes are organized in tandem as a bicistronic operon to regulate synthesis and degradation of c-di-GMP, respectively (*8*). The *dos* gene product is the heme-based oxygen sensor enzyme, *Ec* DOS (*E. coli* direct oxygen sensor), that displays PDE activity toward c-di-GMP in response to O_2 availability (*9*−*14*). The *yddV* gene product has a globin fold domain at the N-terminus and a DGC domain at the C-terminus. Synthesis of c-di-GMP from GTP (DGC) by YddV coupled with degradation of c-di-GMP (PDE) by *Ec* DOS is required for the maintenance of bacterial homeostasis (YddV is designated *Ec* DosC in ref *15*).

[†]This work was partially supported by Special Education and Research Expenses to T.S. and Grants-in-Aid to T.S. (17101002) and T.O. (21570171 and 21350098) from the Ministry of Education, Culture, Sports, Science and Technology of Japan. This work was also supported in part by a Research Fellowship from the Japan Society for the Promotion of Science (JSPS) for Young Scientists to K. Kitanishi.

*To whom correspondence should be addressed: Institute of Multidisciplinary Research for Advanced Materials, Tohoku University, 2-1-1 Katahira, Aoba-ku, Sendai 980-8577, Japan. Telephone: +81-22-217-5604 or -5605. Fax: +81-22-217-5604 or -5390. E-mail: shimizu@tagen.tohoku.ac.jp.

Published on Web 11/10/2010

The globin domain of the YddV protein contains heme, like other well-known heme-bound globin fold proteins, such as myoglobin and hemoglobin. Notably, *Av*GReg, *Bpe*GReg, HemDGC, and HemAT-Bs proteins containing a heme-bound globin domain as the oxygen-sensing site are known globin-coupled oxygen sensor enzymes (*16*−*19*) (Figure 1A). Because the globin-coupled oxygen sensor protein structures and signal transduction mechanisms differ from those of other oxygen sensor types, such as FixL and *Ec* DOS, which contain the heme-bound PAS fold domain (*20*), it is important to explore the oxygen sensing mechanisms of these enzymes. However, only the protein structures of the heme-bound globin domain of HemAT from *Bacillus subtilis* (*16*) and GCS from *Geobacter sulfurreducens* (*21*) have been determined to date. The crystal structures of the six-coordinated Fe(III)−cyanide complex of the isolated heme-bound domain of HemAT (Figure 1B) indicate that His123 is the heme axial ligand at the proximal side and Tyr70 forms electrostatic interactions with the cyanide anion at the heme distal side (*16*). GCS forms a bis-His six-coordinated Fe(III) complex distinct from other globin-coupled oxygen sensor proteins with the five-coordinated structure (*21*). A putative five-coordinated structure of the heme binding site of YddV was proposed, based on the amino acid sequence alignment of globin fold proteins and the structure of the cyanide-bound HemAT-Bs complex (Figure 1B). There is speculation that His98 is the heme axial ligand at the proximal side while Tyr43 and Gln60 at the heme distal side are critical in oxygen binding and sensing of YddV (Figure 1A) [note the following correlations: His98 of YddV = His123 of HemAT-Bs, Tyr43 of YddV = Tyr70 of HemAT-Bs, and Gln60 of YddV = Leu92 of HemAT-Bs (cf. Figure 1B)].

An earlier report about the well-coupled YddV (DGC) and *Ec* DOS (PDE)-mediated regulation of c-di-GMP homeostasis showed that the turnover number of YddV was significantly lower than that of *Ec* DOS (*15*). However, detailed catalytic analysis of YddV has not been performed, because the differences in turnover numbers of the gas-bound and gas-free forms and Fe(III) and Fe(II) forms of YddV remain to be established. In this study, we determined the catalytic properties of YddV under various heme conditions for the first time. The Fe(III), Fe(II)−O_2, and Fe(II)−CO complexes of YddV are active forms with turnover numbers of >0.022 min^{-1}, whereas Fe(II) and Fe(II)−NO complexes are inactive forms. Surprisingly, the YddV turnover number was markedly lower than that (61 min^{-1}) of *Ec* DOS (*9*). It appears the YddV reaction is the rate-determining step for c-di-GMP homeostasis and thus critical for regulating various physiological functions of bacteria.

We further explored the molecular mechanism of O_2 recognition by heme in YddV, based on the amino acid sequence alignment of the globin-coupled oxygen sensor proteins and crystal structure of HemAT. Physicochemical studies of proteins mutated at Tyr43 and Gln60 suggest that (1) Tyr43 is located at the heme distal side and forms hydrogen bonds with the oxygen molecule bound to the Fe(II) complex and (2) this residue is critical for O_2 binding and stability (to prevent iron oxidation) of the Fe(II)−O_2 complex. The partial involvement of Gln60 in stabilization of the Fe(II)−O_2 complex is additionally implied.

EXPERIMENTAL PROCEDURES

Materials. c-di-GMP was obtained from BIOLOG (Bremen, Germany) and 6-(2-hydroxy-1-methyl-2-nitrosohydrazino)-*N*-methyl-1-hexanamine (NOC9) from Sigma. 5-Aminolevulinic acid (5-ALA) was purchased from COSMO BIO (Tokyo, Japan). Other chemicals acquired from Wako Pure Chemical Industries (Osaka, Japan) were of the highest guaranteed grade available and used without further purification. Oligonucleotides were synthesized by Nippon Gene Research Laboratories Inc. (Sendai, Japan) or the Life Sciences Division of Sigma-Aldrich Japan K.K. (Sapporo, Japan).

Cloning of the yddV Gene and Construction of Expression Plasmids. Genomic DNA was isolated from *E. coli* strain K-12 using the Genomic DNA isolation kit (Promega, Madison, WI). The *yddV* gene was amplified by PCR using chromosomal DNA as a template and the following primers: forward, 5′-GTGATAAAG**CATATG**GAGATGTAT-3′; reverse, 5′-CTAATA**GGATCC**CTAAAGACTGGC-3′. Restriction sites are shown in bold, and the stop codon is underlined. PCR products were digested with *Nde*I and *Bam*HI and subcloned into pET28a (Novagen, Darmstadt, Germany), leading to the introduction of a His_6 tag and thrombin cleavage site at the N-terminus of the desired protein. The pET28a-yddV construct was digested with *Nde*I and *Xho*I and subcloned into pET21c (Novagen), thus introducing a His_6 tag at the C-terminus of the desired protein.

Construction of the Isolated Heme-Binding Domain of YddV (*YddV-heme*). To generate the isolated heme domain of YddV (residues 1−153), we inserted a stop codon followed by a *Bam*HI restriction site between positions 153 and 154 of pET28a-yddV, using the Quik Change site-directed mutagenesis kit from Stratagene (La Jolla, CA). The plasmid was digested with *Bam*HI, self-ligated, and sequenced. The following primers were used for mutagenesis: forward, 5′-GGAAGTGATGACTCGC-TA**GGATCC**GCGTTTACCTTTAGTG-3′; reverse, 5′-CAC-TAAAGGTAAACGC**GGATCC**TAGCGAGTCATCACTTCC-3′ (the *Bam*HI site is bold, and the stop codon is underlined).

Site-Directed Mutagenesis. Mutagenesis was conducted using the PrimeSTAR mutagenesis basal kit from Takara Bio (Otsu, Japan). The presence of the desired mutations was confirmed by DNA sequencing. The oligonucleotides employed are listed in Table S1 of the Supporting Information.

Overexpression and Purification of Full-Length YddV Protein. The full-length wild-type YddV protein was expressed

[1]Abbreviations: c-di-GMP, bis(3′−5′)-cyclic dimeric guanosine monophosphate; l-di-GMP, linear di-GMP or pGpG; PDE, phosphodiesterase; GGDEF domain, amino acid sequence that characterizes diguanylate cyclase; EAL domain, amino acid sequence that characterizes PDE; DGC, diguanylate cyclase; PAS, an acronym formed from Per (*Drosophila* period clock protein)-Arnt (vertebrate aryl hydrocarbon receptor nuclear translocator)-Sim (*Drosophila* single-minded protein); *Ec* DOS, *Escherichia coli* direct oxygen sensor or heme-regulated phosphodiesterase from *E. coli*; YddV, heme-bound diguanylate cyclase or c-di-GMP synthase from *E. coli*; SW Mb, sperm whale myoglobin; *Bpe*GReg, globin-coupled oxygen sensor enzyme with the DGC activity from *Bordetella pertussis*; *Av*GReg, globin-coupled oxygen sensor enzyme with the DGC activity from *Azotobacter vinelandii*; HemAT-Bs, globin-coupled oxygen sensor enzyme from *Bacillus subtilis*; HemDGC, heme-containing diguanylate cyclase from *Desulfotalea psychrophila*; FixL, heme-based oxygen sensor histidine kinase that regulates nitrogen fixation in *Rhizobium meliloti* or *Bradyrhizobium japonicum*; YddV-heme, isolated heme-bound globin domain of YddV; *Ec* DOS-PAS, isolated heme-bound PAS domain of *Ec* DOS; Fe(III), Fe(III)−protoporphyrin IX complex, Fe(III) heme complex, or hemin; Fe(II), Fe(II)−protoporphyn IX complex or Fe(II) heme complex; HPLC, high-performance liquid chromatography; NOC9, 6-(2-hydroxy-1-methyl-2-nitrosohydrazino)-*N*-methyl-1-hexanamine; CD, circular dichroism; GAF, domain conserved in cyclic GMP-specific and stimulated phosphodiesterases, adenylate cyclases, and *E. coli* formate hydrogenase transcriptional activator; GCS, globin-coupled sensor; PDB, Protein Data Bank.

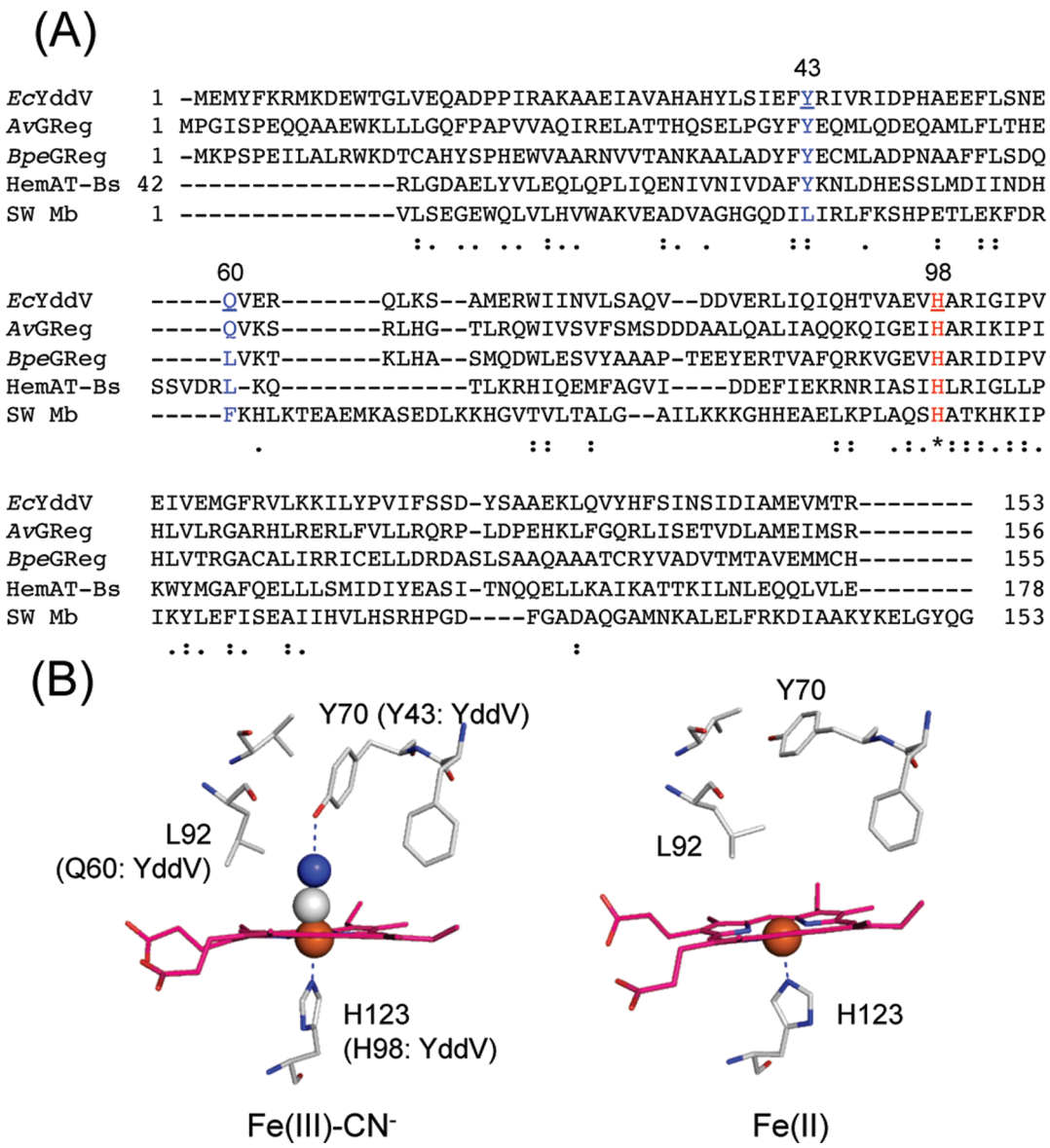

FIGURE 1: (A) Amino acid sequences of relevant heme-bound globin proteins. (B) Heme environmental structures of the Fe(III)−CN^- complex (left, PDB entry 1OR6) and Fe(II) complex (right, PDB entry 1OR4) of HemAT (*16*). We assume that His98 (His123 in HemAT) is the proximal ligand while Tyr43 (Tyr70 in HemAT) and Gln60 (Leu92 in HemAT) are located at the heme distal side in YddV. SWISS-MODEL (http://swissmodel.expasy.org) was used for homology modeling. Although the recognition of Y43 and Q60 as heme distal residues depends solely on alignment with Y70 and L92 of HemAT and the supposed analogy between Q60 and L92 is rather weak (because the residues are bracketed by several gaps), SWISS-MODEL allocated Q60 to the heme distal side.

in *E. coli* Rosetta 2(DE3)pLysS (Novagen) harboring the pET21c(+) expression vector. Briefly, *E. coli* Rosetta 2(DE3)pLysS was transformed with the required plasmid, plated on LB agar containing 100 μg/mL ampicillin and 34 μg/mL chloramphenicol, and incubated at 37 °C overnight. The following day, a single colony was inoculated in LB containing 100 μg/mL ampicillin and 34 μg/mL chloramphenicol and shaken overnight at 200 rpm and 37 °C. The culture medium was added to LB (1:1000 dilution) containing the antibiotics listed above and the mixture shaken at 120 rpm and 37 °C. At an OD_{600} of 1.2, the medium was cooled to 15 °C, and protein expression was induced via addition of 0.1 mM isopropyl β-D-thiogalactopyranoside and 0.45 mM 5-ALA, followed by further shaking for 20 h. *E. coli* cells were harvested by centrifugation for 10 min at 6750*g* and 4 °C, frozen in liquid nitrogen, and stored at −80 °C until they were purified.

E. coli cells frozen at −80 °C were suspended in buffer A [20 mM Tris-HCl (pH 8.0), 150 mM NaCl, and 20 mM imidazole], 1 mM phenylmethanesulfonyl fluoride, and 1 mM EGTA. The solution was sonicated and centrifuged at 100000*g* for 30 min. Supernatant fractions were applied to the Ni-NTA agarose (Qiagen) column. YddV fractions were eluted with a linear gradient from 20 to 300 mM imidazole in buffer A. The YddV-containing solution was dialyzed against 10 mM sodium phosphate (pH 7.4) (buffer B) and concentrated with Centriprep (Millipore, Billerica, MA). Freshly prepared proteins were used for catalytic and spectral analyses. Concentrations were determined using the Coomassie Brilliant Blue dye binding method for protein (Nacalai Tesque, Kyoto, Japan) and the pyridine hemochromogen method for heme. Purified proteins were >95% homogeneous, as confirmed using sodium dodecyl sulfate−polyacrylamide gel electrophoresis.

The purification procedures for the wild-type and mutant YddV-heme proteins were similar to those for full-length YddV protein. See the Supporting Information for details.

Enzymatic Assays. DGC activity was assayed at 30 °C in a reaction mixture containing 10 mM sodium phosphate (pH 7.4), 1 mM $MgCl_2$, 0.2 mM GTP, and 5 μM enzyme. The reaction was terminated when the mixture was heated at 95 °C for 10 min. To determine DGC activity, high-performance liquid chromatography (HPLC) was conducted essentially as described previously (*9*). The nucleotide peaks corresponding to c-di-GMP, GTP, GDP, GMP, and pGpG were verified by coelution with standard samples.

Because the catalytic turnover numbers of YddV were quite low, we needed to identify the species existing as the catalytically active form during experiments over a time period of more than 90 min. We continuously monitored the optical absorption spectra of the Fe(III), Fe(II), Fe(II)−O_2, Fe(II)−CO, and Fe(II)−NO complexes for longer time periods (> 90 min) under conditions similar to those used to obtain the catalytic activities of these complexes.

Optical Absorption Spectra. Absorption spectral data were obtained under aerobic conditions using UV-2500PC and UV-2550PC (Shimadzu, Kyoto, Japan) spectrophotometers. Anaerobic spectral experiments were conducted on a Shimadzu UV-1600PC or UV-1650PC spectrophotometer in a glovebox at N_2 and O_2 concentrations of < 50 ppm (*9*). Following reduction of heme with sodium dithionite, excess dithionite was removed using a Sephadex G-25 column (GE Healthcare, Buckinghamshire, U.K.) in the glovebox. To ensure that the appropriate temperature of the solution was maintained, the reaction mixture was incubated for 10 min, prior to spectroscopic measurements. The Fe(II) complex was prepared in N_2-saturated buffer. Fe(II)−O_2 and −CO complexes were prepared in O_2- and CO-saturated buffers, respectively. Gas-saturated solutions were obtained by bubbling buffers with the appropriate gas for at least 30 min at room temperature (*9*). The NO gas solution was prepared using the NO donor NOC9 (*9*).

Pulse Radiolysis. O_2 and CO association rate constants were obtained using pulse radiolysis. Experiments were performed using a linear accelerator at the Institute of Scientific and Industrial Research, Osaka University (*22*, *23*). The pulse width and energy were 8 ns and 27 MeV, respectively. The light source for the spectrophotometer was a 200 W Xe lamp. After the light had passed through the optical path, transmitted light intensities were analyzed and monitored with a fast spectrophotometric system composed of a Nikon monochromator, an R-928 photomultiplier (Nikon, Tokyo, Japan), and a Unisoku (Osaka, Japan) data analyzing system. The resolution time of the spectrometer was 10 ns. YddV solutions contained 0.1 M *tert*-butyl alcohol (for scavenging of OH radicals) in 10 mM phosphate buffer (pH 7.4) and were deoxygenated via repeated evacuation and flushing with argon in a sealed quartz cuvette. We prepared samples containing O_2 or CO by mixing deoxygenated samples with the appropriate volume of air- or CO-saturated solutions, respectively. The quartz cells had optical path lengths of 1 cm. The sample temperature was maintained at 25 °C. Addition of 0.1 M *tert*-butyl alcohol did not affect the optical absorption spectra of YddV. O_2 binding and CO binding were monitored between 0 and 1 s. Ligand binding was analyzed within this time scale using the following equation:

$$\Delta A(t) = \alpha e^{-kt} \quad (1)$$

where ΔA is the total intensity change at a certain time, t, after pulse radiolysis, α represents the initial intensity, and k represents the rate constant. Association rate constants (k_{on}) were obtained by dividing k by the O_2 (130 μM) or CO concentration (1 mM).

O_2 and CO Dissociation Rate Constants. To determine the O_2 dissociation rate constant, O_2-bound YddV was mixed with anaerobic buffer containing 5 mM dithionite in an RSP-1000 stopped-flow spectrometer (Unisoku) at 25 °C. The CO dissociation rate constant was estimated by mixing CO-bound YddV with NO buffer containing 1 mM dithionite, using a MultiSpec1500 (Shimadzu) spectrometer at 25 °C (*24*, *25*).

As it is possible that NO reacts with dithionite, we measured the CO dissociation rate constant by an additional method using potassium ferricyanide. In brief, CO-bound YddV was admixed with 0.1 mM potassium ferricyanide (*48*). We obtained the same values that were obtained using the NO method. Thus, even if it is possible that NO may interact with dithionite, the CO dissociation rate constants obtained by the NO method do not appear to be significantly different from those obtained by the ferricyanide test, under our experimental conditions. Also, we conducted the same experiments (i.e., using both the NO and ferricyanide tests) on sperm whale myoglobin, as a control experiment. We obtained values very similar to those previously reported (*31*, *48*). Thus, we believe that the methods employed are appropriate.

Autoxidation Rate Constants. To estimate the autoxidation rate constants, solutions of YddV and YddV-heme proteins (containing 5−10 μM heme) were reduced with sodium dithionite in 50 mM Tris-HCl (pH 8.0) containing 1 mM EDTA. Excess dithionite was removed in the glovebox using a Sephadex G-25 column. After removal, the protein solution was mixed with air-saturated buffer to form the Fe(II)−O_2 complex in a cuvette. Changes in UV−visible spectra were monitored with respect to time at 25 °C on UV-2500PC and UV-2550PC (Shimadzu) spectrometers (*24*, *25*).

Determination of the Kinetic Parameters of Cyanide and Imidazole Binding to Wild-Type and Mutant YddV-Heme Proteins. To estimate the ligand association rates, we monitored spectral changes in the heme of YddV-heme after the addition of cyanide or imidazole, as described previously (*25*, *26*). We assume that the ligand−YddV-heme complex is generated via a pseudo-first-order reaction ($v = k_{obs}$[YddV-heme], and $k_{obs} = k_{on}$[ligand] + k_{off}, where [YddV-heme] is significantly lower than [ligand]). As the actual time course for the change in heme absorbance induced by cyanide binding to wild-type and mutant proteins exhibited monophasic kinetics, the observed rate constant (k_{obs}) was obtained by fitting to an exponential function: $\Delta A = A \exp(-k_{obs}t)$. The plots of k_{obs} versus [ligand] exhibited a linear relationship, leading to calculation of k_{on} values for each phase via the equation $k_{obs} = k_{on}$[ligand] + k_{off}. For imidazole binding, absorbance changes of wild-type and all mutant proteins exhibited monophasic kinetics. Thus, the equilibrium dissociation constant (K_d) was obtained by fitting to the hyperbolic function $\Delta A = (AK_d + B[\text{ligand}])/(K_d + [\text{ligand}])$.

Cyanide dissociation experiments were performed via dilution of the cyanide-bound heme protein (30−50 mM cyanide and 5−10 μM heme) solution into 1 mL of buffer. Prior to the reaction, excess cyanide was separated from the YddV-heme−Fe(III)−CN complex using a Sephadex G-25 desalting chromatography column. Because cyanide association reactions of the YddV-heme proteins occur, 100 mM imidazole was added to the reaction buffer to prevent rebinding of cyanide. All dissociation reactions followed pseudo-first-order reaction kinetics. Accordingly, dissociation rates were calculated by curve fitting to a single-exponential function.

Resonance Raman Spectra. Resonance Raman scattering was excited at 413.1 nm with a Kr^+ laser (Spectra Physics, BeamLok 2060) or 441.6 nm with a HeCd laser (Kimmon Koha, IK5651R-G), dispersed with a polychromator (SPEX 1877, 1200 grooves/mm grating), and detected with a liquid nitrogen-cooled CCD detector (CCD-1024×256-OPEN-1LS, HORIBA Jobin Yvon). The laser power of the sample was 3.2 mW for the Fe(III) and Fe(II) complexes, 0.8 mW for the Fe(II) and Fe(II)−CO complexes, and 2.0 mW for the Fe(II)−O_2 complex of YddV-heme. Raman shifts were calibrated with acetone as a frequency standard. The accuracy of the peak position of well-defined Raman bands was ±1 cm^{-1}. The protein concentration was approximately 40 μM in 50 mM Tris-HCl (pH 8.0).

CD Spectra. CD spectra were recorded with a Jasco J-720 CD spectropolarimeter (*27*, *28*).

Redox Potentials. Redox potential values were obtained essentially according to previous protocols (*27*−*29*). Anaerobic spectral experiments were performed in the glovebox using a Shimadzu UV-1650PC spectrometer and a DKK-TOA (Tokyo, Japan) RM-20P portable digital ORP meter equipped with an $Ag^{2+}/AgCl_2$ microelectrode (DKK-TOA). Spectral experiments were performed with 10 μM protein in 0.1 M phosphate buffer (pH 7.0) and 0.1 M NaCl at 15 °C. Prior to titration, 2,3,5,6-tetramethylphenylenediamine (276 mV, 10 μM), *N*-ethylphenazonium ethosulfate (55 mV, 10 μM), and 2-hydroxy-1,4-naphthaquinone (−152 mV, 10 μM) were added to samples as mediators.

RESULTS

Amino Acid Sequences and Hypothetical Structure of the Putative Heme Binding Site. Gene analysis of *yddV* supports the presence of a GGDEF (amino acid motif) domain with DGC function at the C-terminus and a globin domain at the N-terminus. Because the heme-bound globin domain is the oxygen binding site, characterization of the heme binding site associated with O_2 binding and heme redox potential is important for clarifying the molecular mechanism of O_2-enhanced or redox-dependent catalysis of YddV. A hypothetical structure of the globin domain surrounding the heme cofactor of YddV was proposed, based on the sequences and structures of HemAT (*16*) (Figure 1B). We suggest that His98 is a heme axial ligand at the proximal side while Tyr43 and Gln60 located on the heme distal side are critical for recognition or binding of the O_2 molecule (Figure 1A). To establish the roles of these residues in catalysis and protein structure, we further generated His98, Tyr43, and Gln60 mutant proteins and examined their catalytic and spectroscopic properties.

Catalytic Activity of the Purified Full-Length YddV Protein. While YddV displays DGC activity under aerobic conditions, its turnover number under various conditions has not been evaluated to date (*15*). In our experiments, the Fe(III), Fe(II)−O_2, and Fe(II)−CO complexes displayed DGC activity toward GTP, leading to the generation of c-di-GMP with turnover numbers of 0.066, 0.022, and 0.022 min^{-1}, respectively, whereas no significant activity was observed with the Fe(II) and Fe(II)−NO complexes (Table 1 and Figure 2). The autoxidation rate of the full-length enzyme was 0.0092 min^{-1} (Table 2), which was sufficiently high to hinder estimation of the exact turnover number of the Fe(II)−O_2 complex after 90 min. Moreover, because of the instability of the Fe(II)−CO complex, evaluation of the exact turnover number was unfeasible after 90 min. We and another group observed coupling of YddV with *Ec* DOS (a PDE acting on c-di-GMP) to generate pGpG from GTP under aerobic conditions (Figure S1 of the Supporting Information) (*15*). However, the turnover numbers (> 0.022 min^{-1}) of the active forms of YddV were markedly lower than that of active *Ec* DOS (61 min^{-1}) (*9*), suggesting that the DGC reaction of YddV is the rate-determining step for maintaining c-di-GMP homeostasis.

Catalytic Activities of the Mutant Enzymes. Catalytic assays on mutant enzymes did not yield reproducible results when

Table 1: Catalytic Activities in Terms of the Initial Rate of Product Formation (micromoles of c-di-GMP per micromole of YddV per minute) of the Fe(III), Fe(II), Fe(II)−O_2, Fe(II)−CO, and Fe(II)−NO Complexes of Wild-Type Full-Length YddV Proteins[a]

Fe(III)	0.066 ± 0.011 min^{-1}[b]
Fe(II)	< 0.001 min^{-1}
Fe(II)−O_2	0.022 ± 0.003 min^{-1}[c]
Fe(II)−CO	0.022 ± 0.004 min^{-1}[c]
Fe(II)−NO	< 0.001

[a]Experiments were performed at least three times. [b]Activities were evaluated from initial data obtained for up to 90 min. [c]Activities were evaluated from initial data obtained for up to 90 min, because optical absorption spectra indicate that the coordination structures of the Fe(II)−O_2 and Fe(II)−CO complexes are converted to other forms after this time point.

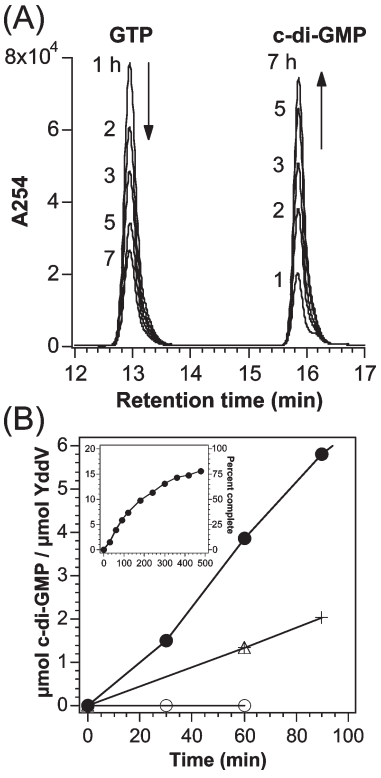

FIGURE 2: Catalytic activity of full-length YddV. (A) HPLC patterns for the time-dependent decrease in the level of GTP and simultaneous increase in the level of c-di-GMP catalyzed by the Fe(III) complex of the full-length YddV enzyme. Data were obtained 1, 2, 3, 5, and 7 h after initiation of the reaction. (B) Time-dependent increase in the level of c-di-GMP over a short time period induced by Fe(III) (●), Fe(II) (○), Fe(II)−O_2 (△), and Fe(II)−CO (+) complexes of the full-length YddV enzyme. No activity was observed with the Fe(II)−NO complex. Evaluation of the exact turnover numbers after 90 min was not feasible for the Fe(II)−O_2 and Fe(II)−CO complexes because of their lack of stability over an extended time range, which is evident from the optical absorption spectral changes of the catalytic solution (cf. Experimental Procedures). The inset depicts the activity of the Fe(III) complex over a longer time period.

Table 2: Autoxidation Rate Constants of the Fe(II)−O_2 Complexes of YddV and Other Heme Proteins[a]

	k_{ox} (min^{-1})	references
wild-type full-length YddV	0.0092	this work
YddV-heme		
WT	0.0076	this work
	0.04	*15*
Y43A	nd[b]	this work
Y43L	nd[b]	this work
Y43F	0.069	this work
Y43W	0.12	this work
Q60A	0.012	this work
Q60E	0.028	this work
Q60L	0.0011	this work
full-length *Ec* DOS	0.015	*24*
PAS domain of *Ec* DOS	0.0058	*24*, *25*
Rm FixL	0.022	*33*
Bj FixL	0.045	*30*
HemAT-Bs	0.001	*32*
SW Mb	0.001	*31*

[a]Experiments were performed at least three times. [b]The Fe(II)−O_2 complex was not formed in the presence of O_2 (260 μM) because of the low oxygen affinity (cf. Table 4). Instead, direct conversion from the Fe(II) to the Fe(III) complex was observed under these conditions.

purified proteins were employed, because protein solutions developed turbidity or the enzymes precipitated. Therefore, we overexpressed mutant proteins in *E. coli* and examined the effects on biofilm formation. In this test, the activities of H98A, H223A, R365A, Tyr43 mutants, and Gln60 mutants were the same as that of the wild-type enzyme (Figure S2 of the Supporting Information). However, the mutant proteins D368A, D376A, and E377A (all mutated at the catalytic active site) lacked biofilm formation activity (Figure S2 of the Supporting Information), thus showing that use of this assay was appropriate for indirectly demonstrating the presence or absence of catalytic activity in mutant enzymes. Therefore, the results suggest that the activity of YddV does not require the presence of the regulatory heme cofactor (H98A mutant) or the putative distal residues Tyr43 and Gln60.

Optical Absorption Spectra of YddV Proteins. The spectrum of Fe(III)-bound purified full-length YddV contained a Soret band at 394 nm and a charge transfer band at 651 nm, suggestive of a five-coordinated high-spin complex (Table S2 of the Supporting Information). No pH-dependent spectral changes were evident within a pH range of 6−10. This eliminates the possibility that the axial ligand in the distal heme side is water or OH^-, confirming the presence of a five-coordinated high-spin Fe(III) complex. The Fe(II) complex was five-cordinated high-spin, whereas Fe(II)−O_2, −CO, and −NO complexes were six-coordinated low-spin complexes, as shown previously (*15*).

Isolation of the heme-bound domain of YddV (YddV-heme) led to slight changes in the optical absorption spectra of the Fe(III) complex. Specifically, wavelengths of the Soret band shifted from 394 to 392 nm and the charge transfer band from 651 to 644 nm. Spectra of the Fe(II), Fe(II)−O_2, and Fe(II)−CO complexes remained unaltered (Figure S3 and Table S2 of the Supporting Information).

Optical absorption spectroscopy studies revealed the loss of heme binding ability in the H98A mutant protein, consistent with the theory that His98 is an axial ligand at the proximal side proposed on the basis of amino acid sequences and reported heme environmental structures of heme-bound globin proteins (Figure 1A,B). However, optical absorption spectra of four Tyr43 and three Gln60 mutant proteins were essentially similar to those of the wild type, except for Y43A and Y43L proteins (Figure S3 and Table S2 of the Supporting Information). Interestingly, conventional spectroscopic and pulse radiolysis data revealed that the Y43A and Y43L mutant proteins essentially lost O_2 binding affinity, and mixing of the O_2 solution with the Fe(II) complex of Y43A or Y43L mutant proteins led to rapid conversion from the Fe(II) to Fe(III) complex (Table 2).

Autoxidation Rate Constants of YddV Proteins. The autoxidation curve representing the shift from the Fe(II)−O_2 complex to Fe(III)-bound full-length YddV comprised a single phase with a rate constant of 0.0092 min^{-1} (Table 2). A comparable value was obtained with YddV-heme. Notably, the rate constants of the YddV proteins were lower than those of full-length *Ec* DOS and FixL proteins (0.015−0.045 min^{-1}) but higher than those of HemAT-Bs and SW Mb (*30*−*33*). The rate constants of the Y43F and Y43W proteins were significantly higher than that of the wild type, while those of Q60A and Q60E mutant proteins were not as high as those of the Tyr mutant proteins (Table 2). The autoxidation rate of the Q60L mutant protein was lower than that of the wild-type counterpart. Our results suggest that Tyr43 plays a more significant role than Gln60 in stabilizing the Fe(II)−O_2 complex of YddV-heme.

O_2 Association and Dissociation Rate Constants of YddV Proteins. Pulse radiolysis experiments involve the instantaneous generation of hydrated electrons (e_{aq}^-), which, in turn, reduce the heme iron of hemoproteins and are thus employed to evaluate O_2 association rate constants (*22*, *23*). The second-order rate constant for O_2 association with the full-length enzyme, composed of a single phase, was evaluated as 0.9 μM^{-1} s^{-1} (Table 3). The rate constant of O_2 dissociation, determined using the stopped-flow method, was composed of a single phase (13 s^{-1}; Table 3). The equilibrium dissociation constant calculated from these rate constants was 14 μM. Isolation of the heme-bound domain (YddV-heme) did not significantly affect the rate constant values.

The Y43F, Y43W, Q60A, and Q60E mutations led to markedly enhanced O_2 dissociation, but not association rate constants (Table 3). Conversely, the Q60L mutation decreased the O_2 dissociation rate constant by 5-fold. As shown above, Y43F, Y43W, Q60A, and Q60E mutations enhanced the autoxidation rate constant. In contrast, the Q60L mutation induced a significant decrease in the autoxidation rate constant (Table 2). Thus, Tyr43 and Gln60 appear to be critical in the O_2 binding and stability of the Fe(II)−O_2−YddV-heme protein complex.

CO Association and Dissociation Rate Constants of YddV Proteins. The CO association and dissociation curves of the full-length enzyme were both composed of a single phase with rate constants of 0.22 μM^{-1} s^{-1} and 0.021 s^{-1}, respectively (Table 3).

Association and dissociation rate constants for CO were not significantly altered by the Tyr43 and Gln60 mutations, except in the case of Y43F, which displayed a 14-fold lower dissociation rate constant than the wild-type protein (Table 3).

Kinetics of Binding of Cyanide to the Tyr43 and Gln60 Mutant Proteins. Optical absorption spectra of the Fe(III)−cyanide complex of the wild-type YddV-heme protein were typical of a six-coordinated low-spin species. Mutations at Tyr43 and Gln60 did not affect the spectral features of the Fe(III) or Fe(III)−cyanide complexes, and thus, heme environment structures of the Fe(III)−cyanide complexes of mutant proteins were essentially similar to those of the wild-type protein. Association

Table 3: O_2 and CO Association and Dissociation Rate Constants of Wild-Type and Mutant YddV and Other Heme Proteins[a]

	k_{on} ($\mu M^{-1} s^{-1}$)	k_{off} (s^{-1})	K_d (μM)[b]	references
		O_2		
wild-type full-length YddV	0.9	13	14	this work
YddV-heme				
WT	1.4	22	16	this work
	3.2	18	9.7	*15*
Y43A	nd[c]	nd[c]	nd[c]	this work
Y43L	nd[c]	nd[c]	nd[c]	this work
Y43F	4.6	53	12	this work
Y43W	4.6	> 150	> 33	this work
Q60A	3.5	39	11	this work
Q60E	1.7	> 80	> 47	this work
Q60L	1.1	4.0	3.6	this work
*Av*GReg		10.6		*18*
*Bpe*GReg	7.0	4.5	0.64	*19*
full-length *Ec* DOS	0.0019	0.64	340	*24*
PAS domain of *Ec* DOS	0.031	0.61	20	*24*
Bj FixL	0.14	20	140	*30*
HemAT-Bs	32	23	0.72	*32*
SW Mb	17	15	0.88	*31*
		CO		
full-length YddV	0.22	0.021	0.095	this work
YddV-heme				
WT	0.40	0.027	0.068	this work
	0.13	0.080	0.64	*15*
Y43A	0.20	0.048	0.24	this work
Y43L	0.32	0.024	0.075	this work
Y43F	0.28	0.0015	0.0054	this work
Y43W	0.27	0.016	0.059	this work
Q60A	0.18	0.040	0.22	this work
Q60E	0.31	0.047	0.15	this work
Q60L	0.25	0.019	0.076	this work
*Av*GReg	1	4	4	*18*
*Bpe*GReg	1.03	0.056	0.055	*19*
full-length *Ec* DOS	0.00081	0.0025	3.1	*24*
PAS domain of *Ec* DOS	0.0078	0.0045	0.58	*24*
Bj FixL	0.005	0.045	9.0	*30*
HemAT-Bs	0.34	0.067	0.20	*35*
SW Mb	0.51	0.019	0.037	*31*

[a]Experiments were performed at least three times. [b]The K_d value was calculated from k_{on} and k_{off} values. [c]The Fe(II)−O_2 complex was not formed because of the low oxygen affinity.

rate constants of cyanide with wild-type and mutant proteins were obtained (Table 4). Notably, the association rate constants of the Tyr43 and Gln60 mutant proteins were not significantly different from that of the wild-type protein, except for Y43W (Table 4). It appears that introduction of Trp, a relatively large amino acid, into position 43 leads to significant disruption of cyanide binding, probably by inducing steric hindrance at the ligand access channel (or the ligand binding pathway from the protein surface to the heme distal side). Introduction of Phe at the same position reduced the cyanide binding rate constant by half (Table 4).

In contrast to association rate constants, the cyanide dissociation rate constant values of mutant proteins obtained in the presence of 100 mM imidazole were substantially larger than that of the wild type, except for that of Q60L (Table 4). For example, the dissociation rate constant of Y43A was > 350-fold higher while those of other mutants were more than 4-fold higher than that of the wild type (with the exception of Q60L). Consequently,

Table 4: Kinetic Parameters of Binding of Cyanide and Imidazole to Wild-Type and Mutant YddV and Other Heme Proteins[a]

Cyanide				
	k_{on} ($M^{-1} s^{-1}$)	k_{off} ($\times 10^{-6} s^{-1}$)	K_d (μM)[b]	references
YddV-heme				
WT	1.8	8.4	4.7	this work
	2.8	17	6.1	*15*
Y43A	1.1	> 3000	> 270	this work
Y43F	0.88	77	87	this work
Y43W	< 0.28	480	> 170	this work
Q60A	1.7	37	22	this work
Q60E	1.2	83	70	this work
Q60L	2.0	3.7	1.9	this work
full-length *Ec* DOS	30	nd		*26*
PAS domain of *Ec* DOS	42	120	2.9	*25*
PAS domain of *Rm* FixL	27	100	4.6	*41*
SW Mb	320	400	1.3	*40*

Imidazole				
	k_{on} ($mM^{-1} s^{-1}$)	k_{off} (s^{-1})[c]	K_d (mM)	References
YddV-heme				
WT	13	0.72	0.055	this work
	5.0		0.075	*15*
Y43A	47	11	0.24	this work
Y43F	14	1.3	0.092	this work
Y43W	2.4	3.8	1.6	this work
Q60A	20	1.2	0.061	this work
Q60E	24	3.2	0.13	this work
Q60L	19	2.1	0.11	this work
full-length *Ec* DOS	0.32	0.77	2.4	*26*
PAS domain of *Rm* FixL	50	100	2.0	*41*
SW Mb	0.13	3.7	28	*52*

[a]Experiments were performed at least three times. [b]Calculated from k_{on} and k_{off} values. [c]Calculated from k_{on} and K_d values.

the equilibrium dissociation constants of the Y43A and Y43W proteins were significantly larger than that of the wild-type protein (by more than 36-fold). Because the effects of Tyr43 mutations on the cyanide dissociation rate constants and equilibrium dissociation constants were more significant than those of Gln60 mutations, we propose that the hydrogen bond interactions of the phenolic hydroxyl group of Tyr43 with the cyanide ion are important for stabilization of the Fe(III)−cyanide complex or inhibition of dissociation of cyanide from the Fe(III) complex.

Kinetics of Binding of Imidazole to the Tyr43 and Gln60 Mutant Proteins. Optical absorption spectra of the Fe(III)−imidazole wild-type YddV-heme complexes were typical of six-coordinated low-spin species. Mutations at Tyr43 and Gln60 did not alter the spectral features of the Fe(III) and Fe(III)−imidazole complexes, indicating that the heme environment structures of the Fe(III)−imidazole complexes of the mutant proteins were essentially similar to those of the wild-type protein.

To obtain the imidazole binding rate constants, we examined the spectral changes following the addition of imidazole to YddV-heme using a stopped-flow spectrometer. As summarized in Table 4, association rate constants of imidazole for Tyr43 and Gln60 mutant proteins were similar to that of the wild-type protein, except in the case of Y43W. The introduction of Trp, a

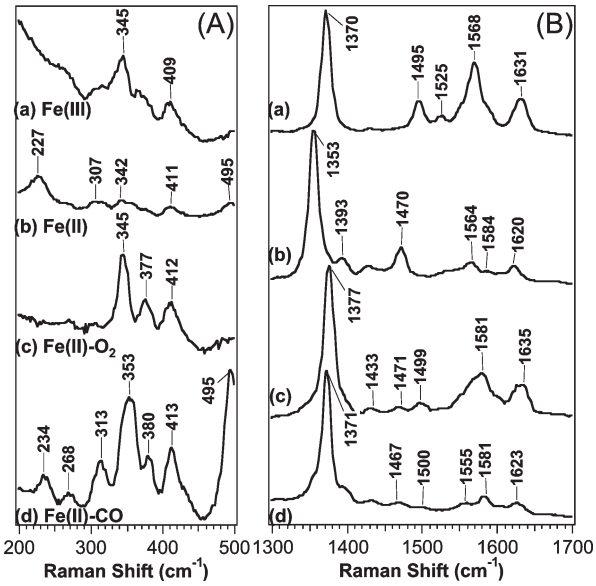

FIGURE 3: Resonance Raman spectra of the Fe(III) (a), Fe(II) (b), Fe(II)−O_2 (c), and Fe(II)−CO (d) complexes of wild-type YddV-heme in the low-frequency (A) and high-frequency regions (B). The excitation wavelength was set as 413.1 nm. Band frequencies are summarized in Table 5.

large residue, at position 43 possibly caused significant steric hindrance, leading to a lower association rate constant for Y43W. We determined equilibrium dissociation constants by monitoring spectral changes following the addition of imidazole to the wild-type and mutant proteins (Figure S4 of the Supporting Information). The equilibrium dissociation constant for the Y43W mutant was 30-fold larger than those of wild-type and other mutant proteins (Table 4). The dissociation rate constant of imidazole calculated from the association rate constants and equilibrium dissociation constant for the Y43A protein was 15-fold larger than that of the wild-type protein, while those of other Tyr43 and Gln60 mutant proteins were only slightly larger than that of the wild-type protein (Table 4 and Figure S1 of the Supporting Information). The data collectively suggest that the effects of Tyr43 and Gln60 mutations on imidazole binding kinetics are less significant than those on cyanide binding kinetics of the protein.

Resonance Raman Spectra of YddV-Heme. Resonance Raman spectra of the Fe(III), Fe(II), Fe(II)−O_2, and Fe(II)−CO complexes of YddV-heme are depicted in Figure 3. The high frequencies of marker bands representing spin state and coordination number are summarized in Table 5 (*36*, *37*). The coordination states of the heme iron based on Raman shifts of these complexes, presented in the right-hand column, are consistent with the coordination structures of complexes suggested from optical absorption spectra.

Difference resonance Raman spectra in the low-frequency region for $^{16}O_2 - {}^{18}O_2$ of the (A) Fe(II)−O_2 complex (Figure 4) and $^{12}C^{16}O - {}^{13}C^{18}O$ of the (B) Fe(II)−CO complex (Figure 5) of YddV-heme proteins are shown in Figure 6. The lower frequencies of stretching modes of the Fe(II)−O_2 and Fe(II)−CO complexes assigned from isotope-sensitive frequencies are summarized in Table 6.

The frequencies of the Fe−His, Fe−O_2, Fe−CO, and C−O stretching modes of Y43F and Q60A mutant proteins are additionally summarized in Table 6. The ν_{Fe-O_2} (565 cm^{-1}), ν_{Fe-CO} (495 cm^{-1}), and ν_{C-O} (1965 cm^{-1}) values of the wild-type protein

Table 5: Resonance Raman Frequencies of the Spin State and Coordination Marker Bands for YddV-Heme in Various Heme States

	ν_2 (cm^{-1})	ν_3 (cm^{-1})	ν_4 (cm^{-1})	heme state[a]
Fe(III)	1568	1495	1370	5cHS
Fe(II)	1564	1470	1353	5cHS
Fe(II)−O_2	1581	1499	1377	6cLS
Fe(II)−CO	1581	1500	1371	6cLS

[a]5cHS, five-coordinated high-spin state; 6cLS, six-coordinated low-spin state.

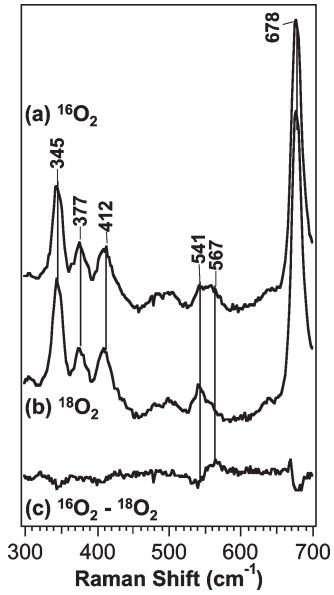

FIGURE 4: Resonance Raman spectra of the Fe(II)−O_2 complex of YddV-heme in the low-frequency region with excitation at 413.1 nm. Spectra of complexes with $^{16}O_2$ (a) and $^{18}O_2$ (b) and their difference spectrum ($^{16}O_2 - {}^{18}O_2$) (c) are depicted.

were shifted to 559, 505, and 1959 cm^{-1}, respectively, for the Y43F mutant protein, implying that both O_2 and CO molecules electrostatically interact with Tyr43. Moreover, small but significant spectral differences in the ν_{Fe-CO} bands of Fe(II)−CO complexes were observed between the wild-type (peak at 499 cm^{-1} and trough at 482 cm^{-1}) and Q60A (peak at 496 cm^{-1} and trough at 480 cm^{-1}) protein spectra (Figure 6). These resonance Raman spectral frequencies indicate that Gln60 also interacts with the CO molecule to an extent.

We measured the resonance Raman spectra of the Fe(II)−O_2 wild-type protein complex in D_2O to determine the impact of H−D exchange on ν_{Fe-O_2} (*58*). However, no frequency shift was detected. This is reminiscent of the behavior of O_2 complexes of cobalt-bound hemoglobin and cobalt-bound myoglobin; these complexes show no frequency shift in D_2O, although the O_2 molecule forms a hydrogen bond with the distal histidine (*59*). Thus, we presently have no direct evidence that O_2 interacts with Tyr43 via a hydrogen bond.

CD Spectrum of YddV-Heme. The α-helix content of YddV-heme was evaluated as 79−85%, based on the CD band in the far-UV region (Table S3 of the Supporting Information) (*39*). Conversely, the β-sheet content was very low (≤11%).

Redox Potential of YddV-Heme. The redox potential of YddV-heme was evaluated as −17 mV versus the standard hydrogen electrode (SHE) (Table 7). We suggest that the Fe(III) complex is slightly more stable than the Fe(II) complex.

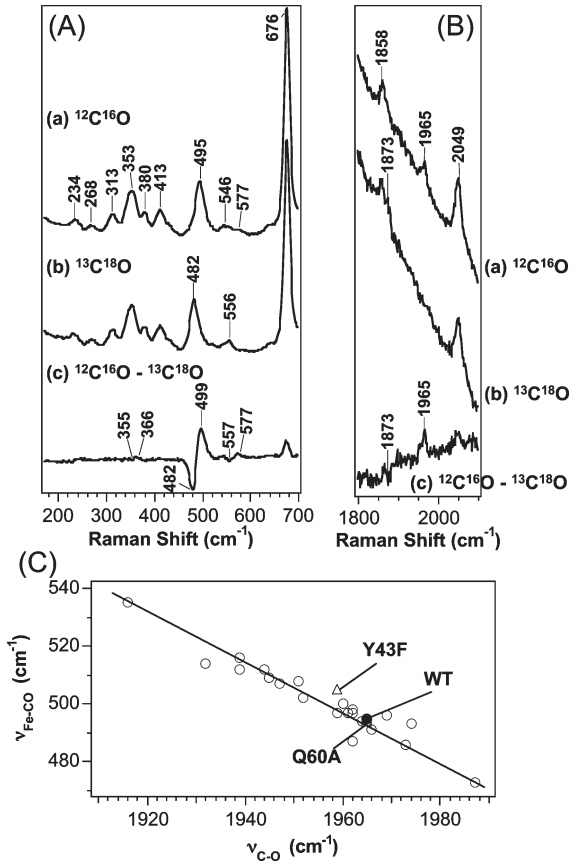

FIGURE 5: Resonance Raman spectra of the Fe(II)−CO complex of YddV-heme in the low-frequency (A) and high-frequency (B) regions with excitation at 413.1 nm. Spectra of complexes with $^{12}C^{16}O$ (a) and $^{13}C^{18}O$ (b) and their difference spectrum ($^{12}C^{16}O$ − $^{13}C^{18}O$) (c) are shown in panels A and B. An inverse correlation plot between ν_{Fe-CO} and ν_{C-O} frequencies of the Fe(II)−CO complex is presented in panel C.

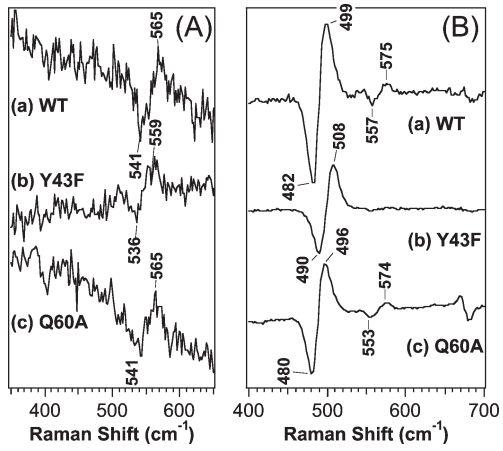

FIGURE 6: Difference resonance Raman spectra representing the differences ($^{16}O_2$ − $^{18}O_2$) in the (A) Fe(II)−O_2 complexes and differences ($^{12}C^{16}O$ − $^{13}C^{18}O$) in the (B) Fe(II)−CO complexes of wild-type and mutant YddV-heme proteins in the low-frequency regions with excitation at 413.1 nm: (a) wild-type, (b) Y43F, and (c) Q60A proteins. Frequencies of the ν_{Fe-O_2}, ν_{Fe-CO}, and ν_{C-O} modes of the wild-type and mutant proteins are summarized in Table 6.

DISCUSSION

In this study, we investigate the active forms [Fe(III), Fe(II)−O_2, and Fe(II)−CO complexes] and inactive forms [Fe(II) and Fe(II)−NO complexes] of the globin-coupled heme-bound oxygen sensor DGC, YddV. The catalytic activities of the active YddV forms were determined to be >0.022 min^{-1}. It appears that the DGC reaction catalyzed by YddV is the rate-determining step for c-di-GMP homeostasis. Spectroscopic analyses of Tyr43 and Gln60 mutant proteins revealed that Tyr43 at the heme distal side in YddV is critical for recognition of the O_2 molecule and stability of the Fe(II)−O_2 complex of the enzyme.

CO and cyanide, nonphysiological diatomic molecular ligands, were used in this study because the association−dissociation kinetics and equilibrium dissociation constants of such ligands, binding to heme proteins, yield valuable information about the ligand access channel and the heme distal environment (*12*−*16*, *24*−*28*, *31*, *36*, *37*, *40*, *48*). Although imidazole is not diatomic, spectroscopic studies have shown that imidazole sensitively probes steric hindrance in the distal pocket of a heme protein (*52*). Use of both nonphysiological ligands, and physiological O_2, is thus essential for gaining a fundamental understanding of protein molecular mechanisms.

Optical Absorption Spectra, Ligand Kinetics, and Autoxidation. The spectra of both Fe(III) and Fe(II) complexes of YddV are characteristic of a five-coordinated high-spin form. A similar five-coordinated Fe(III) complex was obtained via introduction of Val or Leu into the heme distal cavity of human myoglobin in lieu of His64 of the oxygen-interacting site via site-directed mutagenesis and removal of the water molecule from the distal side (*52*).

The O_2 binding rate and equilibrium dissociation constants of YddV imply that the O_2 molecule binds to YddV less favorably, compared to globin proteins (*30*−*32*). These unfavorable O_2 binding characteristics may be used to regulate oxidation from the inactive Fe(II) to active Fe(III) and Fe(II)−O_2 forms.

The Y43A and Y43L mutations induced a significant decrease in O_2 affinity (Table 3). It appears that O_2 binding is controlled by steric or hydrophobic characteristics of the ligand access channel rather than electrostatic characteristics at the heme distal side.

Evaluation of the autoxidation rate constant for each complex is important, because the Fe(III) complex has higher activity than the Fe(II)−O_2 complex (Figure 2 and Table 1), and the autoxidation rate constant reflects the rate of conversion from the Fe(II)−O_2 to the Fe(III) complex (Table 2). The autoxidation rate of the heme iron complex is associated with the electrostatic characteristics or polarities of the environment of the complex, redox potentials of iron, and electrostatic characteristics of porphyrin (*24*, *25*).

The autoxidation rate of YddV was additionally markedly increased upon mutation of Tyr43. The Gln60 mutations led to altered O_2 dissociation and autoxidation rate constants (Tables 2 and 3) but had no significant effects on the O_2 and CO association rate constants. Ligand dissociation (but not association) behavior is reflected by resonance Raman spectra, consistent with kinetic data on mutant proteins, as discussed below. It appears that interactions between ligands and Gln60 exist but are not as strong as those of Tyr43.

The autoxidation rate constant (0.0011 min^{-1}) of Q60L Ydd-heme is significantly lower than that (0.0076 min^{-1}) of the wild-type protein in contrast to other mutant proteins, which display rate constants significantly higher than that of the wild-type protein (Table 2). *Bpe*GReg, a globin-coupled oxygen sensor, contains Leu at the Gln60 site of YddV. The presence of the hydrophobic residue at this site may be additionally important for the stability of the Fe(II)−O_2 complex. The relatively low redox potential value (−17 mV vs SHE) of YddV-heme, compared with those of *Ec* DOS, hemoglobin, and myoglobin, supports this proposal (Table 7).

Table 6: Frequencies of the Fe−His, Fe−O_2, Fe−CO, and C−O Stretching Modes of Wild-Type, Y43F, and Q60A YddV-Heme and Other Heme-Bound Globin Proteins

	ν_{Fe-His} (cm^{-1})	ν_{Fe-O_2} (cm^{-1})	ν_{Fe-CO} (cm^{-1})	ν_{C-O} (cm^{-1})	references
YddV-heme					
WT	227	565	495	1965	this work
Y43F	227	559	505	1959	this work
Q60A	227	565	494	1965	this work
HemAT-Bs					
WT	225	566	494	1964	*32*
Y70F		566	494	1961	*43*
HemDGC					
WT	226	566	506	1944	*42*
Y55F			506		*42*
Q81A			496		*42*
SW Mb	220	569	507	1947	*36*−*38*, *44*
Mt Hb[a]	226	560	500, 535	1960, 1916	*34*, *45*
Pc Hb[b]	220	563	493	1974	*46*
Ascaris Hb		566	515, 543	1909, 1948	*47*

[a] *Mt* Hb, *Mycobacterium tuberculosis* hemoglobin. [b] *Pc* Hb, *Paramecium caudatum* hemoglobin.

Table 7: Redox Potentials (millivolts vs SHE) of YddV-Heme and Other Heme Proteins[a]

	reductive	oxidative	references
YddV-heme	−17 (n = 0.95)	−27 (n = 1.1)	this work
Ec DOS-PAS	63	70	*25*, *27*, *28*
Aplysia Mb (pH 6.0)	137		*48*
SW Mb (pH 6.0)	55		*48*
horseradish peroxidase	−250		*49*
cytochrome $P450_{cam}$	−300		*50*
cytochrome b_{562}	113		*51*
cytochrome *c*	260		*29*

[a] Experiments were performed twice, and experimental certainties were calculated with the n value.

Interactions between Cyanide Anion and the Phenolic Hydroxyl Group of Tyr43. For HemeAT, electrostatic interactions exist between the cyanide anion and the phenolic hydroxyl group of Tyr70 (corresponding to Tyr43 of YddV) (Figure 1B) (*16*). The results of cyanide binding kinetics of Tyr43 mutant proteins of YddV-heme confirm that interactions between the cyanide anion and the phenolic hydroxyl group of Tyr43 are important for Fe(III)−cyanide complex stability, as suggested for the Fe(II)−O_2 complex. However, steric factors are possibly important for imidazole binding, because the effects of the Y43W mutation on imidazole binding are more significant than those of Y43A.

The cyanide and O_2 binding kinetics of Tyr43 mutant proteins of the Fe(III) and Fe(II) complexes are similar. In addition, both Fe(III) and Fe(II) complexes of YddV maintain the five-coodinated high-spin structure. Therefore, for globin-coupled oxygen sensor proteins, no substantial structural changes should occur in the heme distal side upon the redox switch. This mechanism is distinct from that of the PAS protein in that global structural changes (in particular, those at the heme distal side) occur when the Fe(III) complex is reduced to the Fe(II) complex for heme-bound PAS proteins (*10*, *11*, *13*, *14*).

The catalytic activity of *Ec* DOS, a heme-regulated oxygen sensor enzyme, is substantially enhanced by the binding of external ligands, such as cyanide or imidazole, to the Fe(III) form (*26*). However, heavy precipitates were formed upon addition of these ligands to the Fe(III) complex, which hampered estimation of catalytic activity.

Resonance Raman Spectroscopy. The Fe−O_2 frequency (ν_{Fe-O_2}) (565 cm^{-1}) of YddV-heme is analogous to those of *Pc* Hb (563 cm^{-1}) and *Ascaris* Hb (566 cm^{-1}) (*32*, *34*, *46*, *47*). For these Hbs, the distal O atom of the O_2 molecule bound to the Fe(II) heme complex forms hydrogen bonds with residues at the heme distal side, which is also possible in YddV. The marked change in the Y43F mutant spectrum suggests that Tyr43 directly interacts with the O_2 molecule bound to the Fe(II) heme complex of YddV-heme, as depicted in Figure 1B. Another hypothesis is that the distal structure of the Y43F mutant protein is similar to those of L29F/H64Q double SW Mb and elephant myoglobin mutant protein (*53*), which contain a large aromatic residue in the oxygen binding site at the distal side of the heme protein.

In DevS, an effect of D_2O on ν_{Fe-O_2} was observed (*58*), suggesting that the hydroxyl group of tyrosine interacts, at the heme distal side, with the proximal oxygen atom of the O_2 molecule bound to the heme iron. However, in YddV, no effect of D_2O on ν_{Fe-O_2} was apparent, suggesting that the hydroxyl group of Tyr43, again at the heme distal side, interacts rather with the distal oxygen atom of the O_2 molecule. In myoglobin, the imidazole of histidine interacts with the distal oxygen atom of the O_2 molecule bound to the heme iron and no effect of D_2O on ν_{Fe-O_2} is apparent, but an effect of D_2O on ν_{O-O} is observed in the cobalt−myoglobin−O_2 complex [cobalt-bound myoglobin was used because ν_{O-O} cannot be detected in an Fe(II)−O_2 complex] (*59*). In YddV, although we could not obtain direct evidence of the interaction between the hydroxyl group of Tyr43 and the distal oxygen atom using the H−D exchange experiments of resonance Raman spectroscopy, it is nonetheless suggested that such interaction exists, based on ligand kinetic data and the autoxidation rate constants of the Tyr43 mutant proteins. Also, the difference in ν_{Fe-O_2} between the wild-type (565 cm^{-1}) and Y43F (559 cm^{-1}) proteins supports this proposal.

The Fe−CO frequency (495 cm^{-1}) of YddV-heme is close to those of HemAT-Bs (494 cm^{-1}) and *Pc* Hb (493 cm^{-1}). Moreover, the C−O frequency (1965 cm^{-1}) of YddV-heme is similar to that of HemAT-Bs (1964 cm^{-1}). The Y43F mutation led to marked alterations in these frequencies (Table 6), suggesting that Tyr43 interacts with the CO molecule bound to the Fe(II) heme complex. This result is consistent with the finding that the CO dissociation rate constant is decreased 20-fold (Table 3), possibly because the ligand dissociation rate constant reflects the

coordination structure of the static state (as evident from resonance Raman spectra) in contrast to the ligand association rate constant, which reflects the environment of the ligand access channel.

Notably, the Y70F mutation in HemAT did not affect the Fe−O_2, Fe−CO, or C−O stretching modes (Table 6). Additionally, the Y55F mutation in HemDGC did not affect the Fe−CO stretching mode (Table 6). Therefore, it should be emphasized that YddV-heme is the only globin-coupled heme-based oxygen sensor protein in which critical roles of Tyr at the heme distal side in O_2 and CO recognition and/or interactions have been unequivocally confirmed with the aid of resonance Raman spectroscopy.

We cannot definitively conclude that the mutations changed the frequencies (traces b and c in Figure 6) of the δ_{Fe-C-O} bands (557 and 577 cm^{-1}) observed for the wild-type protein (trace a in Figure 6). Rather, the disappearance of these bands from the Y43F spectrum suggests that the CO molecule binds the Fe(II) heme complex more linearly in the mutant protein. The proposal is based on the finding that the δ_{Fe-C-O} band is not activated in unhindered (or linear) heme−CO adducts of the myoglobin−CO complex, and its intensity is possibly an indication of off-axis CO binding in response to steric hindrance (*38*). The Fe(II)−CO complex is more stable [high affinity of CO for the Fe(II) heme complex] when CO binds the Fe(II) heme complex in a linear manner (*31*). Therefore, resonance Raman data are consistent with the low rate of dissociation of CO from the Y43F mutant protein (Table 3).

Catalytic Activities of the Mutant Enzymes. The catalytic biofilm formation activities of mutant enzymes, assessed in vivo, suggest that oxygen binding and/or the heme redox state of YddV would be critical for enzyme activity under unusual or extreme conditions. We speculate that the following mechanism is used. On the basis of the existence of an in vitro coupling reaction involving both the Fe(III) forms of YddV and *Ec* DOS (Figure S1 of the Supporting Information), YddV would constitutively and slowly (0.066 min^{-1}) synthesize c-di-GMP. In contrast, *Ec* DOS would regulate the concentration of c-di-GMP, with a high turnover number (8−70 min^{-1}), thus rapidly exerting phosphodiesterase activity in response to environmental stimuli. This implies that c-di-GMP homeostasis in bacteria is controlled principally by the activity of *Ec* DOS. The relatively fast autoxidation rate constant reflects the instability of the Fe(II)−O_2 complex of YddV. Thus, bacterial YddV would in fact be in equilibrium between the active Fe(III) form and the inactive Fe(II) form, because the lifetime of the Fe(II)−O_2 complex is rather short. Under hypoxic or reductive conditions, YddV would assume the inactive Fe(II) form and terminate the synthesis of c-di-GMP. In the H98A variant strain, the heme-free form of YddV remains active and YddV is also active in the distal mutant proteins. YddV would need heme to suppress catalysis under such conditions. It could be subsequently concluded that the heme regulatory role is to act as the catalytic inhibitor or repressor. A similar role in catalytic control for the heme iron of *Ec* DOS has been suggested. Thus, the heme-free form of *Ec* DOS also shows high-level catalytic activity, suggesting that heme is supplied to the sensor domain to suppress catalysis (*26*).

Summary. In this study, we evaluate the turnover numbers of a heme-bound globin-coupled DGC, YddV, from *E. coli*. The Fe(III) and Fe(II)−O_2 complexes are active forms (turnover numbers of >0.022 min^{-1}), whereas the Fe(II) complex is the inactive form of the enzyme. Therefore, the DGC reaction of YddV is the rate-determining step for the two consecutive reactions involving conversion of GTP to pGpG via c-di-GMP catalyzed by YddV and *Ec* DOS (turnover number of 61 min^{-1}) for the maintenance of c-di-GMP homeostasis. Spectral data on the putative heme environment of the mutant proteins suggest that His98 is the proximal axial ligand to the heme iron (Figure 1A,B), while Tyr43 and Gln60 located at the heme distal side form electrostatic interactions with the O_2 molecule bound to the Fe(II) heme complex. In particular, the importance of Tyr43 in the O_2 recognition and stability of the Fe(II)−O_2 complex is highlighted. Moreover, we propose that subtle tuning of the redox switch of the heme iron complex appears to be important for the regulation of catalysis, based on the redox potential value (−17 mV vs SHE) of the heme of YddV. The overall protein structure of the heme binding globin domain appears to be similar to that of HemAT-Bs. Interestingly, heme-based oxygen sensor proteins with different protein folds, such as the GAF domain, also contain Tyr as the O_2-interacting site on the heme distal side (*54*−*58*).

ACKNOWLEDGMENT

We are grateful to Mr. Hiroto Takahashi and Dr. Yasuyuki Araki for helping with the HPLC experiments and ligand binding kinetics, respectively, in the initial stages of this study. We also thank Dr. Fumi Nagatsugi for allowing access to the CD spectrometer and Dr. Teizo Kitagawa (University of Hyogo) for invaluable discussions.

SUPPORTING INFORMATION AVAILABLE

Expression and purification procedures of YddV-heme, oligonucleotides used for construction of expression vectors for mutant proteins, optical absorption spectral maxima, contents of α-helix, β-sheet, and turns evaluated with CD spectra, coupling reaction of YddV and *Ec* DOS, optical absorption spectra of YddV-heme, imidazole binding, biofilm formation, and amino acid sequences of the middle and DGC domains. This material is available free of charge via the Internet at http://pubs.acs.org.

REFERENCES

1. Hengge, R. (2009) Principles of c-di-GMP signalling in bacteria. *Nat. Rev. Microbiol. 7*, 263–273.
2. Schirmer, T., and Jenal, U. (2009) Structural and mechanistic determinants of c-di-GMP signaling. *Nat. Rev. Microbiol. 7*, 724–735.
3. Simm, R., Morr, M., Kader, A., Nimtz, M., and Römling, U. (2004) GGDEF and EAL domains inversely regulate cyclic di-GMP levels and transition from sessility to motility. *Mol. Microbiol. 53*, 1123–1134.
4. Jonas, K., Edwards, A. N., Simm, R., Romeo, T., Römling, U., and Melefors, O. (2008) The RNA binding protein CsrA controls cyclic di-GMP metabolism by directly regulating the expression of GGDEF proteins. *Mol. Microbiol. 70*, 236–257.
5. Galperin, M. Y. (2004) Bacterial signal transduction network in a genomic perspective. *Environ. Microbiol. 6*, 552–567.
6. Schmidt, A. J., Ryjenkov, D. A., and Gomelsky, M. (2005) The ubiquitous protein domain EAL is a cyclic diguanylate-specific phosphodiesterase: Enzymatically active and inactive EAL domains. *J. Bacteriol. 187*, 4774–4781.
7. Römling, U., Gomelsky, M., and Galperin, M. Y. (2005) C-di-GMP: The dawning of a novel bacterial signalling system. *Mol. Microbiol. 57*, 629–639.
8. Méndez-Ortiz, M. M., Hyodo, M., Hayakawa, Y., and Membrillo-Hernández, J. (2006) Genome-wide transcriptional profile of *Escherichia coli* in response to high levels of the second messenger 3′,5′-cyclic diguanylic acid. *J. Biol. Chem. 281*, 8090–8099.
9. Tanaka, A., Takahashi, H., and Shimizu, T. (2007) Critical role of the heme axial ligand, Met^{95}, in locking catalysis of the phosphodiesterase from *Escherichia coli* (*Ec* DOS) toward cyclic diGMP. *J. Biol. Chem. 282*, 21301–21307.

10. Park, H., Suquet, C., Satterlee, J. D., and Kang, C. (2004) Insights into signal transduction involving PAS domain oxygen-sensing heme proteins from the X-ray crystal structure of *Escherichia coli* Dos heme domain (*Ec* DosH). *Biochemistry 43*, 2738–2746.
11. Kurokawa, H., Lee, D. S., Watanabe, M., Sagami, I., Mikami, B., Raman, C. S., and Shimizu, T. (2004) A redox-controlled molecular switch revealed by the crystal structure of a bacterial heme PAS sensor. *J. Biol. Chem. 279*, 20186–20193.
12. Sasakura, Y., Yoshimura-Suzuki, T., Kurokawa, H., and Shimizu, T. (2006) Structure-function relationships of *Ec*DOS, a heme-regulated phosphodiesterase from *Escherichia coli*. *Acc. Chem. Res. 39*, 37–43.
13. Gilles-Gonzalez, M. A., and Gonzalez, G. (2005) Heme-based sensors: Defining characteristics, recent developments, and regulatory hypotheses. *J. Inorg. Biochem. 99*, 1–22.
14. Gilles-Gonzalez, M. A., and Gonzalez, G. (2004) Signal transduction by heme-containing PAS-domain proteins. *J. Appl. Physiol. 96*, 774–783.
15. Tuckerman, J. R., Gonzalez, G., Sousa, E. H. S., Wan, X., Saito, J. A., Alam, M., and Gilles-Gonzalez, M. A. (2009) An oxygen-sensing diguanylate cyclase and phosphodiesterase couple for c-di-GMP control. *Biochemistry 48*, 9764–9774.
16. Zhang, W., and Phillips, G. N., Jr. (2003) Structure of the oxygen sensor in *Bacillus subtilis*: Signal transduction of chemotaxis by control of symmetry. *Structure 11*, 1097–1110.
17. Hou, S., Larsen, R. W., Boudko, D., Riley, C. W., Karatan, E., Zimmer, M., Ordal, G. W., and Alam, M. (2000) Myoglobin-like aerotaxis transducers in Archaea and Bacteria. *Nature 403*, 540–544.
18. Thijs, L., Vinck, E., Bolli, A., Trandafir, F., Wan, X., Hoogewijs, D., Coletta, M., Fago, A., Weber, R. E., Van Doorslaer, S., Ascenzi, P., Alam, M., Moens, L., and Dewilde, S. (2007) Characterization of a globin-coupled oxygen sensor with a gene-regulating function. *J. Biol. Chem. 282*, 37325–37340.
19. Wang, X., Tuckerman, J. R., Saito, J. A., Freitas, T. A. F., Newhouse, J. S., Denery, J. R., Galperin, M. Y., Gozalez, G., Gilles-Gonzalez, M. A., and Alam, M. (2009) Globins synthesize the second messenger bis-(3′-5′)-cyclic diguanosine monophosphate in bacteria. *J. Mol. Biol. 388*, 262–270.
20. Möglich, A., Ayers, R. A., and Moffat, K. (2009) Structure and signaling mechanism of Per-ARNT-Sim domains. *Structure 17*, 1282–1294.
21. Pesce, A., Thijs, L., Nardini, M., Desmet, F., Sisinni, L., Gourlay, L., Bolli, A., Coletta, M., Van Doorslaer, S., Wan, X., Alam, M. Ascenzi, P., Moens, L., Bolognesi, M., and Dewilde, S. (2009) HisE11 and HisF8 provide bis-histidyl heme hexa-coordination in the globin domain of *Geobacter sulfurreducens* globin-coupled sensor. *J. Mol. Biol. 386*, 246–260.
22. Kobayashi, K., Tagawa, S., Daff, S. N., Sagami, I., and Shimizu, T. (2001) Rapid calmodulin-dependent interdomain electron transfer in neuronal nitric-oxide synthase measured by pulse radiolysis. *J. Biol. Chem. 276*, 39864–39871.
23. Nakajima, H., Nakagawa, E., Kobayashi, K., Tagawa, S., and Aono, S. (2001) Ligand-switching intermediates for the CO-sensing transcriptional activator CooA measured by pulse radiolysis. *J. Biol. Chem. 276*, 37895–37899.
24. Taguchi, S., Matsui, T., Igarashi, J., Sasakura, Y., Araki, Y., Ito, O., Sugiyama, S., Sagami, I., and Shimizu, T. (2004) Binding of oxygen and carbon monoxide to a heme-regulated phosphodiesterase from *Escherichia coli*: Kinetics and infrared spectra of the full-length wild-type enzyme, isolated PAS domain, and Met-95 mutants. *J. Biol. Chem. 279*, 3340–3347.
25. Ishitsuka, Y., Araki, Y., Tanaka, A., Igarashi, J., Ito, O., and Shimizu, T. (2008) Arg97 at the heme-distal side of the isolated heme-bound PAS domain of a heme-based oxygen sensor from *Escherichia coli* (*Ec* DOS) plays critical roles in autoxidation and binding to gases, particularly O_2. *Biochemistry 47*, 8874–8884.
26. Tanaka, A., and Shimizu, T. (2008) Ligand binding to the Fe(III)-protoporphyrin IX complex of phosphodiesterase from *Escherichia coli* (*Ec* DOS) markedly enhances catalysis of cyclic di-GMP: Roles of Met95, Arg97, and Phe113 of the putative heme distal side in catalytic regulation and ligand binding. *Biochemistry 47*, 13438–13446.
27. Sasakura, Y., Hirata, S., Sugiyama, S., Suzuki, S., Taguchi, S., Watanabe, M., Matsui, T., Sagami, I., and Shimizu, T. (2002) Characterization of a direct oxygen sensor heme protein from *Escherichia coli*: Effects of the heme redox states and mutations at the heme-binding site on catalysis and structure. *J. Biol. Chem. 277*, 23821–23827.
28. Hirata, S., Matsui, T., Sasakura, Y., Sugiyama, S., Yoshimura-Suzuki, T., Sagami, I., and Shimizu, T. (2003) Characterization of Met95 mutants of a heme-regulated phosphodiesterase from *Escherichia coli*. *Eur. J. Biochem. 270*, 4771–4779.
29. Dutton, P. L. (1978) Redox potentiometry: Determination of midpoint potentials of oxidation-reduction components of biological electron-transfer systems. *Methods Enzymol. 54*, 411–435.
30. Gilles-Gonzalez, M. A., Gonzalez, G., Perutz, M. F., Kiger, L., Marden, M. C., and Poyart, C. (1994) Heme-based sensors, exemplified by the kinase FixL, are a new class of heme protein with distinctive ligand binding and autoxidation. *Biochemistry 33*, 8067–8073.
31. Springer, B. A., Sligar, S. G., Olson, J. S., and Phillips, G. N., Jr. (1994) Mechanisms of ligand recognition in myoglobin. *Chem. Rev. 94*, 699–714.
32. Aono, S., Kato, T., Matsuki, M., Nakajima, H., Ohta, T., Uchida, T., and Kitagawa, T. (2002) Resonance Raman and ligand binding studies of the oxygen-sensing signal transducer protein HemAT from *Bacillus subtilis*. *J. Biol. Chem. 277*, 13528–13538.
33. Tanaka, A., Nakamura, H., Shiro, Y., and Fujii, H. (2006) Roles of the heme distal residues of FixL in O_2 sensing: A single convergent structure of the heme moiety is relevant to the downregulation of kinase activity. *Biochemistry 45*, 2515–2523.
34. Couture, M., Yeh, S.-R., Wittenberg, B. A., Wittenberg, J. B., Ouellet, Y. H., Rousseau, D. L., and Guertin, M. (1999) A cooperative oxygen-binding hemoglobin from *Mycobacterium tuberculosis*. *Proc. Natl. Acad. Sci. U.S.A. 96*, 11223–11228.
35. Zhang, W., Olson, J. S., and Phillips, G. N., Jr. (2005) Biophysical and kinetic characterization of HemAT, an aerotaxis receptor from *Bacillus subtilis*. *Biophys. J. 88*, 2801–2814.
36. Uchida, T., and Kitagawa, T. (2005) Mechanism for transduction of the ligand-binding signal in heme-based gas sensory proteins revealed by resonance Raman spectroscopy. *Acc. Chem. Res. 38*, 662–670.
37. Spiro, T. G., and Li, X.-Y. (1988) in Biological Applications of Raman Spectroscopy (Spiro, T. G., Ed.) Vol. 3, pp 1−37, John Wiley & Sons, New York.
38. Ramsden, J., and Spiro, T. G. (1989) Resonance Raman evidence that distal histidine protonation removes the steric hindrance to upright binding of carbon monoxide by myoglobin. *Biochemistry 28*, 3125–3128.
39. Whitmore, L., and Wallace, B. A. (2004) DICHROWEB, an online server for protein secondary structure analyses from circular dichroism spectroscopic data. *Nucleic Acids Res. 32*, W668–W673.
40. Dou, Y., Olson, J. S., Wilkinson, A. J., and Ikeda-Saito, M. (1996) Mechanism of hydrogen cyanide binding to myoglobin. *Biochemistry 35*, 7107–7113.
41. Winkler, W. C., Gonzalez, G., Wittenberg, J. B., Hille, R., Dakappagari, N., Jabob, A., Gonzalez, L. A., and Gilles-Gonzalez, M. A. (1996) Nonsteric factors dominate binding of nitric oxide, azide, imidazole, cyanide, and fluoride to rhizobial heme-based oxygen sensor FixL. *Chem. Biol. 3*, 841–850.
42. Sawai, H., Yoshioka, S., Uchida, T., Hyodo, M., Hayakawa, Y., Ishimori, K., and Aono, S. (2010) Molecular oxygen regulates the enzymatic activity of a heme-containing diguanylate cyclase (HemDGC) for the synthesis of cyclic di-GMP. *Biochim. Biophys. Acta 1804*, 166–172.
43. Yoshimura, H., Yoshioka, S., Kobayashi, K., Ohta, T., Uchida, T., Kubo, M., Kitagawa, T., and Aono, S. (2006) Specific hydrogen-bonding networks responsible for selective O_2 sensing of the oxygen sensor protein HemAT form *Bacillus subtilis*. *Biochemistry 45*, 8301–8307.
44. Kitagawa, T., Nagai, K., and Tsubaki, M. (1979) Assignment of the Fe-N_ε (His F8) stretching band in the resonance Raman spectra of deoxy myoglobin. *FEBS Lett. 104*, 376–378.
45. Yeh, S. R., Couture, M., Ouellet, Y. H., Guertin, M., and Rousseau, D. L. (2000) A cooperative oxygen binding hemoglobin from *Mycobacterium tuberculosis*: Stabilization of heme ligands by a distal tyrosine residue. *J. Biol. Chem. 275*, 1679–1684.
46. Das, T. K., Weber, R. E., Dewilde, S., Wittenberg, J. B., Wittenberg, B. A., Yamauchi, K., Van Hauwaert, M. L., Moens, L., and Rousseau, D. L. (2000) Ligand binding in the ferric and ferrous states of *Paramecium* hemoglobin. *Biochemistry 39*, 14330–14340.
47. Das, T. K., Friedman, J. M., Kloek, A. P., Goldberg, D. E., and Rousseau, D. L. (2000) Origin of the anomalous Fe-CO stretching mode in the CO complex of *Ascaris* hemoglobin. *Biochemistry 39*, 837–842.
48. Antonini, E., and Brunori, M. (1971) Hemoglobin and myoglobin in their reactions with ligands, North-Holland Publishing Co., Amsterdam.
49. Yamada, H., Makino, R., and Yamazaki, I. (1975) Effects of 2,4-substituents of deuteroheme upon redox potentials of horseradish peroxidases. *Arch. Biochim. Biophys. 169*, 344–353.
50. Sligar, S. G., and Gunsalus, I. C. (1976) A thermodynamic model of regulation: Modulation of redox equilibria in camphor monoxygenase. *Proc. Natl. Acad. Sci. U.S.A. 73*, 1078–1082.

51. Itagaki, E., and Hager, L. P. (1968) The amino acid sequence of cytochrome b_{562} of *Escherichia coli*. *Biochem. Biophys. Res. Commun. 32*, 1013–1019.
52. Mansy, S. S., Olson, J. S., Gonzalez, G., and Gilles-Gonzalez, M. A. (1998) Imidazole is a sensitive probe of steric hindrance in the distal pockets of oxygen-binding heme proteins. *Biochemsitry 37*, 12452–12457.
53. Zhao, X., Vyas, K., Nguyen, B. D., Rajarathnam, K., La Mar, G. N., Li, T., Phillips, G. N., Jr., Eich, R. F., Olson, J. S., Ling, J., and Bocian, D. F. (1995) A double mutant of sperm whale myoglobin mimics the structure and function of elephant myoglobin. *J. Biol. Chem. 270*, 20763–20774.
54. Huan, S. H., Rio, D. C., and Marletta, M. A. (2007) Ligand binding and inhibition of an oxygen-sensitive soluble guanylate cyclase, Gyc-88E, from *Drosophila*. *Biochemistry 46*, 15115–15122.
55. Cho, H. Y., Cho, H. J., Kim, Y. M., Oh, J. I., and Kang, B. S. (2009) Structural insight into heme-based redox sensing by DosS from *Mycobacterium tuberculosis*. *J. Biol. Chem. 284*, 13057–13067.
56. Ioanoviciu, A., Meharenna, Y. T., Poulos, T. L., and Ortiz de Montellano, P. R. (2009) DevS oxy complex stability identifies this heme protein as a gas sensor in *Mycobacterium tuberculosis* dormancy. *Biochemistry 48*, 5839–5848.
57. Podust, L. M., Ioanoviciu, A., and Ortiz de Montellano, P. R. (2008) 2.3 Å X-ray structure of the heme-bound GAF domain of sensory histidine kinase DosT of *Mycobacterium tuberculosis*. *Biochemistry 47*, 12523–12531.
58. Yukl, E. T., Ioanoviciu, A., Nakano, M. M., Ortiz de Montellano, P. R., and Moënne-Loccoz, P. (2008) A distal tyrosine residue is required for ligand discrimination in DevS from *Mycobacterium tuberculosis*. *Biochemistry 47*, 12532–12539.
59. Kitagawa, T., Ondrias, M. R., Rousseau, D. L., Ikeda-Saito, M., and Yonetani, T. (1982) Evidence for hydrogen bonding of bound dioxygen to the distal histidine of oxycobalt myoglobin and haemoglobin. *Nature 298*, 869–871.